Research Article | Vol. 25, No. 5 | 6 Mar 2017 | OPTICS EXPRESS 5156

Optics EXPRESS

Controlling periodic ripple microstructure formation on 4H-SiC crystal with three time-delayed femtosecond laser beams of different linear polarizations

WANLIN HE,[1] JIANJUN YANG,[1,2,*] AND CHUNLEI GUO[2,3]

[1]*Institute of Modern Optics, Nankai University, Tianjin 300071, China*
[2]*Changchun Institute of Optics, Fine Mechanics and Physics, Chinese Academy of Sciences, Changchun 130033, China*
[3]*The Institute of Optics, University of Rochester, Rochester, New York 14627, USA*
[*]*jjyang@nankai.edu.cn*

Abstract: The control of laser-induced periodic ripple microstructures on 4H-SiC crystal surface is studied using temporally delayed collinear three femtosecond laser pulse trains linearly polarized in different directions. The ripple orientation appears to develop independent of the individual laser polarizations and exhibits non-monotonical change with variable time delays, whose variation tendency is also affected by the polarization intersection angles. Remarkably, the ripple period is observed to transfer from high- to low-spatial-frequency regions, accompanied by distinctly improved morphological uniformity and clearness. The results are satisfactorily interpreted based on a physical model of the surface wave excitation on a transient index metasurface, which is confirmed by further experiments. Our investigations indicate that transient noneqilibrium dynamics of the material surface provides an effective way to manipulate the laser-induced microstructures.

OCIS codes: (140.3390) Laser materials processing; (320.7120) Ultrafast phenomena; (310.6628) Subwavelength structures, nanostructures.

References and links

1. M. Birnbaum, "Semiconductor surface damage produced by ruby lasers," J. Appl. Phys. **36**(11), 3688–3689 (1965).
2. Y. Yang, J. Yang, C. Liang, and H. Wang, "Ultra-broadband enhanced absorption of metal surfaces structured by femtosecond laser pulses," Opt. Express **16**(15), 11259–11265 (2008).
3. V. Zorba, E. Stratakis, M. Barberoglou, E. Spanakis, P. Tzanetakis, and C. Fotakis, "Tailoring the wetting response of silicon surfaces via fs laser structuring," Appl. Phys., A Mater. Sci. Process. **93**(4), 819–825 (2008).
4. A. Y. Vorobyev and C. Guo, "Direct femtosecond laser surface nano/microstructuring and its applications," Laser Photonics Rev. **7**(3), 385–407 (2013).
5. Y. Tang, J. Yang, B. Zhao, M. Wang, and X. Zhu, "Control of periodic ripples growth on metals by femtosecond laser ellipticity," Opt. Express **20**(23), 25826–25833 (2012).
6. L. Qi, K. Nishii, and Y. Namba, "Regular subwavelength surface structures induced by femtosecond laser pulses on stainless steel," Opt. Lett. **34**(12), 1846–1848 (2009).
7. R. Wagner, J. Gottmann, A. Horn, and E. W. Kreutz, "Subwavelength ripple formation induced by tightly focused femtosecond laser radiation," Appl. Surf. Sci. **252**(24), 8576–8579 (2006).
8. R. Kuladeep, C. Sahoo, and D. N. Rao, "Direct writing of continuous and discontinuous sub-wavelength periodic surface structures on single-crystalline silicon using femtosecond laser," Appl. Phys. Lett. **104**(22), 222103 (2014).
9. L. Xue, J. Yang, Y. Yang, Y. Wang, and X. Zhu, "Creation of periodic subwavelength ripples on tungsten surface by ultra-short laser pulses," Appl. Phys., A Mater. Sci. Process. **109**(2), 357–365 (2012).
10. A. Y. Vorobyev and C. Guo, "Femtosecond laser-induced periodic surface structure formation on tungsten," J. Appl. Phys. **104**(6), 063523 (2008).
11. D. C. Emmony, R. P. Howson, and L. J. Willis, "Laser mirror damage in germanium at 10.6 μm," Appl. Phys. Lett. **23**(11), 598–600 (1973).
12. M. Huang, F. Zhao, Y. Cheng, N. Xu, and Z. Xu, "Origin of laser-induced near-subwavelength ripples: interference between surface plasmons and incident laser," ACS Nano **3**(12), 4062–4070 (2009).

#283566 https://doi.org/10.1364/OE.25.005156
Journal © 2017 Received 23 Dec 2016; revised 17 Feb 2017; accepted 19 Feb 2017; published 27 Feb 2017

Optics EXPRESS

13. J. Bonse, A. Rosenfeld, and J. Kruger, "On the role of surface plasmon polaritons in the formation of laser-induced periodic surface structures upon irradiation of silicon by femtosecond-laser pulses," J. Appl. Phys. **106**(10), 104910 (2009).
14. F. Garrelie, J. P. Colombier, F. Pigeon, S. Tonchev, N. Faure, M. Bounhalli, S. Reynaud, and O. Parriaux, "Evidence of surface plasmon resonance in ultrafast laser-induced ripples," Opt. Express **19**(10), 9035–9043 (2011).
15. S. Sakabe, M. Hashida, S. Tokita, S. Namba, and K. Okamuro, "Mechanism for self-formation of periodic grating structures on a metal surface by a femtosecond laser pulse," Phys. Rev. B **79**(3), 033409 (2009).
16. X. Wu, T. Jia, F. Zhao, M. Huang, N. Xu, H. Kuroda, and Z. Xu, "Formation mechanisms of uniform arrays of periodic nanoparticles and nanoripples on 6H-SiC crystal surface induced by femtosecond laser ablation," Appl. Phys., A Mater. Sci. Process. **86**(4), 491–495 (2007).
17. J. Reif, O. Varlamova, and F. Costache, "Femtosecond laser induced nanostructure formation: self-organization control parameters," Appl. Phys., A Mater. Sci. Process. **92**(4), 1019–1024 (2008).
18. M. Huang, F. Zhao, Y. Cheng, N. Xu, and Z. Xu, "Mechanisms of ultrafast laser-induced deep-subwavelength gratings on graphite and diamond," Phys. Rev. B **79**(12), 125436 (2009).
19. J. Bonse and J. Krüger, "Pulse number dependence of laser-induced periodic surface structures for femtosecond laser irradiation of silicon," J. Appl. Phys. **108**(3), 034903 (2010).
20. Y. Yang, J. Yang, L. Xue, and Y. Guo, "Surface patterning on periodicity of femtosecond laser- induced ripples," Appl. Phys. Lett. **97**(14), 141101 (2010).
21. X. Li, W. Rong, L. Jiang, K. Zhang, C. Li, Q. Cao, G. Zhang, and Y. Lu, "Generation and elimination of polarization-dependent ablation of cubic crystals by femtosecond laser radiation," Opt. Express **22**(24), 30170–30176 (2014).
22. S. Höhm, M. Herzlieb, A. Rosenfeld, J. Krüger, and J. Bonse, "Formation of laser-induced periodic surface structures on fused silica upon two-color double-pulse irradiation," Appl. Phys. Lett. **103**(25), 254101 (2013).
23. M. Barberoglou, D. Gray, E. Magoulakis, C. Fotakis, P. A. Loukakos, and E. Stratakis, "Controlling ripples' periodicity using temporally delayed femtosecond laser double pulses," Opt. Express **21**(15), 18501–18508 (2013).
24. X. Li, C. Li, L. Jiang, X. Shi, N. Zhang, and Y. Lu, "Ablation area quasiperiodic oscillations in semiconductors with femtosecond laser double-pulse delay," Opt. Lett. **39**(8), 2382–2385 (2014).
25. H. Qiao, J. Yang, F. Wang, Y. Yang, and J. Sun, "Femtosecond laser direct writing of large-area two-dimensional metallic photonic crystal structures on tungsten surfaces," Opt. Express **23**(20), 26617–26627 (2015).
26. J. Kim, S. Na, S. Cho, W. Chang, and K. Whang, "Surface ripple changes during Cr film ablation with a double ultrashort laser pulse," Opt. Lasers Eng. **46**(4), 306–310 (2008).
27. M. Gedvilas, J. Mikšys, and G. Račiukaitis, "Flexible periodical micro- and nano-structuring of a stainless steel surface using dual-wavelength double-pulse picosecond laser irradiation," RSC Advances **5**(92), 75075–75080 (2015).
28. S. Höhm, M. Herzlieb, A. Rosenfeld, J. Krüger, and J. Bonse, "Laser-induced periodic surface structures on fused silica uponcross-polarized two-color double-fs-pulse irradiation," Appl. Surf. Sci. **336**, 39–42 (2015).
29. V. Hommes, M. Miclea, and R. Hergenröder, "Silicon surface morphology study after exposure to tailored femtosecond pulses," Appl. Surf. Sci. **252**(20), 7449–7460 (2006).
30. M. Hashida, T. Nishii, Y. Miyasaka, H. Sakagami, M. Shimizu, S. Inoue, and S. Sakabe, "Orientation of periodic grating structures controlled by double-pulse irradiation," Appl. Phys., A Mater. Sci. Process. **122**(4), 1–5 (2016).
31. Y. Ma, V. Khuat, and A. Pan, "A simple method for well-defined and clean all-SiC nano-ripples in ambient air," Opt. Lasers Eng. **82**, 141–147 (2016).
32. G. Obara, H. Shimizu, T. Enami, E. Mazur, M. Terakawa, and M. Obara, "Growth of high spatial frequency periodic ripple structures on SiC crystal surfaces irradiated with successive femtosecond laser pulses," Opt. Express **21**(22), 26323–26334 (2013).
33. T. Tomita, K. Kinoshita, S. Matsuo, and S. Hashimoto, "Effect of surface roughening on femtosecond laser-induced ripple structures," Appl. Phys. Lett. **90**(15), 153115 (2007).
34. M. Yamaguchi, S. Ueno, R. Kumai, K. Kinoshita, T. Murai, T. Tomita, S. Matsuo, and S. Hashimoto, "Raman spectroscopic study of femtosecond laser-induced phase transformation associated with ripple formation on single-crystal SiC," Appl. Phys., A Mater. Sci. Process. **99**(1), 23–27 (2010).
35. V. Khuat, J. Si, T. Chen, and X. Hou, "Deep-subwavelength nanohole arrays embedded in nanoripples fabricated by femtosecond laser irradiation," Opt. Lett. **40**(2), 209–212 (2015).
36. W. He and J. Yang, "Evidencing ultrafast non-equilibrium dynamics in SiC crystal by femtosecond laser induced slanting surface nanostructures," J. Appl. Phys. (to be published).
37. J. Cong, J. Yang, B. Zhao, and X. Xu, "Fabricating subwavelength dot-matrix surface structures of molybdenum by transient correlated actions of two-color femtosecond laser beams," Opt. Express **23**(4), 5357–5367 (2015).
38. S. J. Elston, G. P. Bryan-Brown, and J. R. Sambles, "Polarization conversion from diffraction gratings," Phys. Rev. B Condens. Matter **44**(12), 6393–6400 (1991).
39. F. J. Garcia-Vidal, L. Martín-Moreno, and J. B. Pendry, "Surfaces with holes in them: new plasmonic metamaterials," J. Opt. A, Pure Appl. Opt. **7**(2), S97–S101 (2005).

Optics EXPRESS

40. J. Chen, W. K. Chen, J. Tang, and P. M. Rentzepis, "Time-resolved structural dynamics of thin metal films heated with femtosecond optical pulses," Proc. Natl. Acad. Sci. U.S.A. **108**(47), 18887–18892 (2011).
41. S. K. Das, H. Messaoudi, A. Debroy, E. McGlynn, and R. Grunwald, "Multiphoton excitation of surface plasmon-polaritons and scaling of nanoripple formation in large bandgap materials," Opt. Mater. Express **3**(10), 1705–1715 (2013).

1. Introduction

Laser-induced periodic surface structures, also so-called ripples, are recognized as a universal phenomenon of the laser-solid interactions ever since the first report by Birnbaum [1], and have gained remarkable attention because of both basic research interests and wide potential applications [2–4]. Compared with continuous and long-pulsed laser irradiations, the ripple structures induced by femtosecond laser pulses can have periods significantly smaller than the laser wavelength, which have been independently evidenced on many kinds of materials, such as metals, dielectric and semiconductors [5–8]. In most cases, the ripple formation is oriented perpendicular to the laser polarization [9,10]. Although different models have been proposed to describe the underlying mechanisms, including the scattering surface electromagnetic waves [11], the excitation of surface-plasmon polaritons [12–14], surface wave induced by parametric decay process [15], second-harmonic generation [16], and self-organization [17], the essential physics are not entirely clear and are still controversial.

Under single beam irradiation conditions, extensive efforts have devoted to manipulate the ripple structures through varying the incident femtosecond laser parameters (such as the central wavelength, the energy fluence, the number of pulses, and the polarization state) [18–21], but the ability to adjust seems to be restricted because the ripple formation processes are essentially predominated by the transient optical properties of the irradiated materials, particularly for dielectrics and semiconductors. In order to take advantage of the material dynamic response, several studies have recently investigated the ripple formation by applying temporally delayed femtosecond double pulses with either cross or parallel polarizations [22–29], in which both the rippled surface area and the structure periodicity were observed to decrease with increasing inter-pulse time delays; moreover, on titanium surface the induced ripple orientation was found slantwise relative to the incident both laser polarizations [30]. In spite of these results, the control of ripple quality still remains a challenge, the physical interpretations are mostly related to the temporal evolution of the carrier density, and the physical influence of the spatially distributed transient dielectric permittivity is of little concern.

In this study, we introduce a novel experimental method by irradiating semiconductor 4H-SiC crystal with sequences of three collinear femtosecond laser pulses of different linear polarizations to comprehensively elucidate the underlying mechanisms of the periodic ripple formation. By varying their time delays, the induced ripple orientation begins to change in a specific range, depending on the time delay between the first and the second laser pulses; whereas the ripple period can be switched from $\Lambda = 0.18\ \lambda$ into a region of $\Lambda = 0.63\sim0.87\ \lambda$ (Λ is the ripple period, λ is the laser wavelength) especially with well-defined profiles, just as with metal surfaces. A physical model based on the femtosecond laser interaction with the transient index metasurface is proposed, which gives additional insights into the nonequilibrium dynamic material changes during the ripple formation. The validity of our theory is not only confirmed by the satisfactory explanations of the observations, but also supported by the further experimental results with alternative intersection angles of three laser polarizations.

2. Experimental

A schematic diagram of the experimental setup is shown in Fig. 1. A commercial chirped pulse amplification of Ti: sapphire laser system (Spectra Physics HP-Spitfire 50) was employed as a light source, which delivers horizontally polarized laser pulse trains at 1 kHz repetition rate with the central wavelength of λ = 800 nm. The time duration and the

Optics EXPRESS

maximum energy of the laser pulse are 50 fs and 2 mJ, respectively. In the experiment, each laser pulse output from the amplifier was divided into three near-energy sub-pulses (P_1, P_2 and P_3) through two beam splitters (BS_1 and BS_2), and the optical delay lines were adopted in the beam paths of P_2 and P_3 to respectively cause a time delay of Δt = 0-60 ps, thus making three laser pulses arrive onto a sample surface by temporal sequence. Moreover, two half-wave plates were inserted in the aforementioned two beam paths to alter their laser polarizations, whereas the linear polarization of the laser beam P_2 is always kept along the horizontal direction. After this, the three femtosecond laser beams of different linear polarizations were spatially superposed into collinear propagation and then focused in air at normal incidence onto the sample surface through a microscope objective lens (4 × , N. A = 0.1). The sample, a single-face polished crystal of 4H-SiC (001) with a thickness of 1mm and the surface roughness of 5 nm, was mounted on a three-axis (xyz) translation stage (NewPort UTM301 PPE1) and placed ~300 μm before the focus, which leads to a Gaussian laser spot diameter (1/e intensity) of approximate 60 μm on the surface. The selection of SiC semiconductor single crystal is motivated by its unique physical properties and potential applications in high temperature electronic devices. The experiments were performed by a line-scribing method, in which the sample was translated at a speed of 0.1 mm/s, resulting in 600 laser pulses partially overlapped within one beam spot area. Before and after the experiments, the sample surface was ultrasonically cleaned in acetone solution. The surface morphologies were observed with scanning electron microscopy (SEM) and atomic force microscopy (AFM). In order to gain a clear understanding of the experimental details, several key parameters should be here defined: θ_1 represents an angle between directions of the electric fields of the laser beams P_1 and P_2, θ_2 for the angle between directions of the electric fields of the laser beams P_3 and P_2, Δt_1 for the time delay between the laser beams P_1 and P_2, and Δt_2 for the time delay between the laser beams P_2 and P_3.

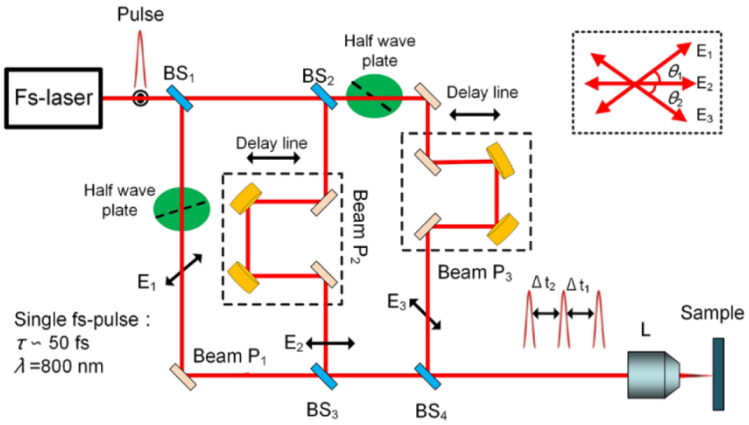

Fig. 1. Schematic diagram of the experimental setup. Abbreviation: BS_1, BS_2, BS_3 and BS_4: beam splitter; fs: femtosecond; E_1, E_2 and E_3: electric fields of the laser beams P_1, P_2 and P_3, respectively; τ: pulse width; λ: center wavelength of the laser; L: microscope objective lens. An inset diagram illustrates the relationships among the linear polarizations of three laser beams P_1, P_2 and P_3.

3. Results and discussions

First, the morphological changes of the sample surface irradiated by the three isolated individual sub-pulse femtosecond laser beams were experimentally investigated, where the peak fluence of each laser beam is 0.24 J/cm^2 and the intersection angles among their linear polarizations are $\theta_1 = \theta_2 = 30°$, and the results are shown in Figs. 2(a)-2(c). In all cases the typical high-spatial-frequency (HSF) ripple structures are observed to form with an identical period of approximately Λ = 150 nm; whereas their spatial orientations are much more

Optics EXPRESS

different but respectively perpendicular to the direction of the corresponding laser polarization due to surface plasmon excitation. In particular, such kinds of HSF ripple structures seem to be cut into short lengths and present a semi-periodic distribution, which is very similar to the previous reports [31, 32].

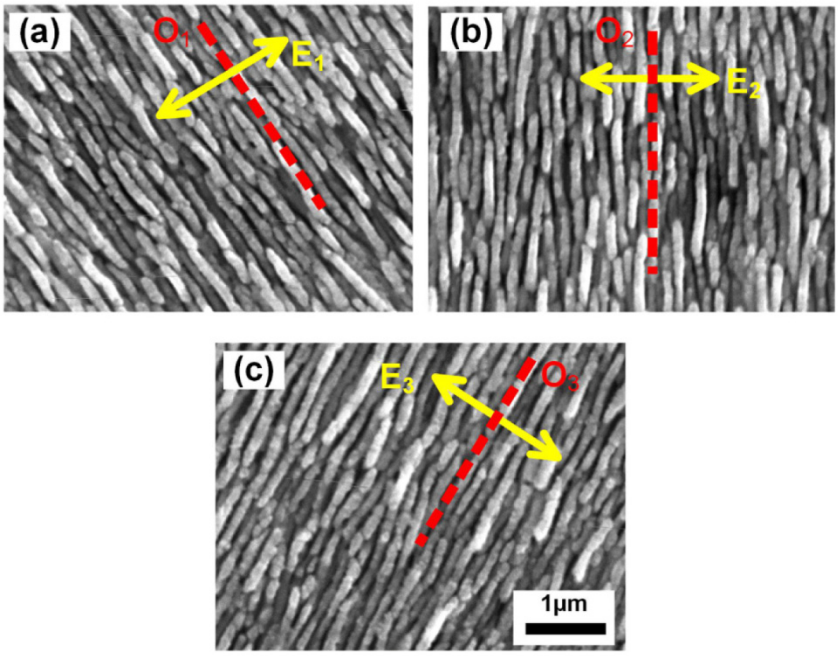

Fig. 2. (a)-(c) SEM images of the HSF ripple structures formed on the surface of 4H-SiC crystal using three isolated individual femtosecond laser beams, which have different linear polarizations with the same peak fluence of 0.24 J/cm^2. Here the yellow double solid arrows denote directions of the electric field (or linear polarization) of the laser beams; while the red dashed lines (O_1, O_2 and O_3) represent the orientations of the laser-induced ripple structures.

For the purpose of experimental comparisons, we began to generate the surface structures under the spatial overlapping irradiation of three time-delayed sub-pulse laser beams. To avoid deteriorating the laser-induced ripple surface structures by the strong ablation process, the peak fluence of three sub-pulse laser beams were simultaneously attenuated to the same value of 0.07 J/cm^2, thus making no periodic surface structures upon irradiation by any one or two pulses. Figure 3 shows the experimental results obtained under the conditions of $\theta_1 = \theta_2 = 30°$, $\Delta t_1 = 10$ ps and $\Delta t_2 = 42$ ps. Namely, with respect to the pulse of the laser beam P_1, the pulses of the laser beams P_2 and P_3 have a respective time delay of 10 ps and 52 ps to arrive onto the target. Clearly, some unique features for the achieved surface structures can be described as follows:

(i) The ripple structures are apparently oriented in a particular direction, which is neither perpendicular nor parallel to any directions of three laser polarizations. Being relative to the ripple orientation induced by the high-intensity laser beam P_3 [which is adopted in the whole paper], the currently obtained ripple orientation undergoes a counter-clockwise slanting degree of $\alpha = 46.6°$. (ii) The length of the ripples can be continuously extended into a long range without breakages, and the structure profiles exhibit the improved morphological clearness. Moreover, the above mentioned SEM image was also investigated by the fast Fourier transformation, and the corresponding result is shown in Fig. 3(d), wherein the distinct bright spots actually reflect the spatial regularity of the structure arrangement. (iii) The topography measurements of AFM reveal that the ripple period increases to about $\Lambda = 680$ nm with a modulation depth of approximate 180 nm. Compared with the situations in

Optics EXPRESS

Fig. 2, the duty ratio of the ripple structures (ridge width to the ripple period) is observed to reduce, which represents the larger groove width during the ripple formation. In general, all these results indicate a fact that the ripple structures induced by the three temporally delayed femtosecond laser pulse beams are likely to transform from a HSF morphology into a low-spatial-frequency (LSF) profile. Another interesting point is that our present LSF ripple structures on the semiconductor seem to be very similar to the observations on metal surfaces [5, 25, 30], but much different from the ripple structures on SiC surface induced by a single femtosecond laser beam [31–35]. [It should be stressed here that in our experiments the slanting behaviors of the ripple orientation are the same on the entire region of the laser-scribed line areas, which is actually independent of the intensity variations on a Gaussian focal spot, and they can be maintained even with different scanning speeds (within a range of 0.01-0.4 mm/s).]

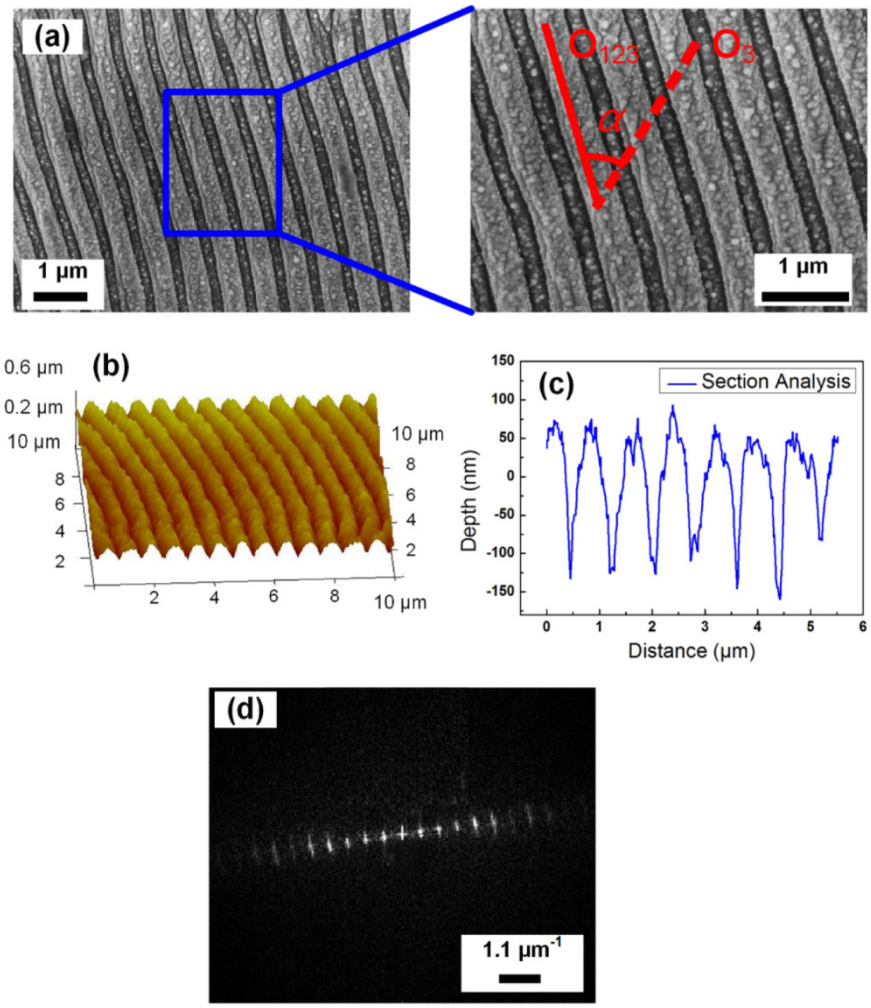

Fig. 3. (a) SEM images of the LSF ripple structures on the surface of 4H-SiC crystal using three temporally delayed (Δt_1 = 10 ps and Δt_2 = 42 ps) collinear femtosecond laser beams, where the peak fluence of each laser beam is 0.07 J/cm^2, and the intersection angles among three laser polarizations are $\theta_1 = \theta_2 = 30°$. The red solid line ($O_{123}$) denotes the ripple orientation induced by three femtosecond laser beams; (b)-(c) AFM image of the LSF periodic surface structures and its cross-section profile line; (d) An image of the fast Fourier transformation (FFT) of Fig. 3 (a).

Optics EXPRESS

To reveal effects of the temporal separation among three femtosecond laser sub-pulses on the formation of the ripple surface structures, we tried to change the second time delay Δt_2 within a range of 0-60 ps by a minimum step of 2 ps, while keeping the first time delay Δt_1 = 10 ps and the polarization intersection angles $\theta_1 = \theta_2 = 30°$. In other words, the laser beam P_1 is earliest to arrive on the target surface, which is then followed by the delayed incident laser beams P_2 and P_3 in the time subsequence. As shown by some typical experimental results in Fig. 4, the morphological profiles of the laser-induced ripple structures are different when varying the second time delay Δt_2. For example, in the case of $\Delta t_2 = 0$ ps, *i.e.*, when the laser beams P_2 and P_3 simultaneously reach the material surface, the ripple structures can be produced with the LSF features with more or less spatial bending profiles. The ripple orientation is observed to slant with a degree of approximate $\alpha = 30°$, which becomes nearly perpendicular to the direction of the linear polarization of the laser beam P_2, or this kind of the alignment is very similar to the observation in Fig. 2(b) but with different spatial period.

With gradually increasing the time delay Δt_2, the available ripple orientation is further slanted counter-clockwise. At $\Delta t_2 = 10$ ps, the LSF ripple structures are surprisingly found to be well-organized into a uniform distinct appearance. Compared with the situation of $\Delta t_2 = 0$ ps, the groove widths appear to be much more evident, indicating a decrease in the duty ratio of the ripple structures. In this case, the measured slanting degree of the ripple orientation is increased to about $\alpha = 42.5°$. If the second time delay continues to increase to $\Delta t_2 = 40$ ps, the high-quality, uniform LSF ripple structures can still be formed, especially with the extendable length and evident morphological clearness, and the measured slanting degree of the ripple orientation becomes approximately $\alpha = 45.5°$. However, when the second time delay is further enlarged to $\Delta t_2 = 60$ ps, the obtained slanting degree of the LSF ripple orientation turns to decrease down to about $\alpha = 40.5°$ rather than continuously increase. On the other hand, the ripple structure quality begins to be degraded.

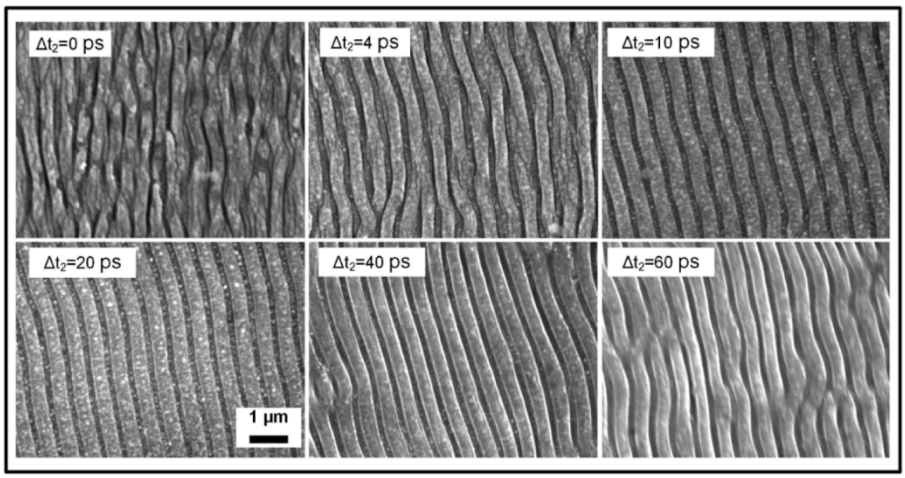

Fig. 4. Observed LSF ripple structures on the surface of 4H-SiC crystal using three femtosecond laser pulse beams with several time delays of Δt_2, where other laser parameters are adopted as $\theta_1 = \theta_2 = 30°$ and $\Delta t_1 = 10$ ps.

Based on the above experimental measurements, a quantitative description of the slanting degree of the ripples orientation in terms of the second time delay Δt_2 is shown in Fig. 5(a), where each data is obtained by averaging three different measurements on the patterned area of the sample surface, and the error bar represents a standard deviation of 5%. Clearly, under the condition of Δt_1 = 10 ps, with continuously increasing Δt_2, there are non-monotonic variations in the measured ripple orientation angle, *i.e.*, during a time-delay range of Δt_2 = 0-42 ps it is likely to grow from near $\alpha = 30°$ to a maximum value of about $\alpha = 46.6°$, and then

Optics EXPRESS

become slightly decreased for the larger time delays. Figure 5(b) displays the evolution of both the ripple period and the duty ratio with the second time delay Δt_2. It can be seen that the ripple period firstly undergoes a rapidly increasing tendency from Λ = 518 nm to 707 nm and then remains almost invariant. With regard to the measured time-delay dependence of the duty ratio of the ripple structures, its values seem to be almost unchangeable at 0.72 except for the case of Δt_2 = 0 ps. Figure 5(c) shows variations of the ripple depth as a function of the second time delay. Clearly, at Δt_2 = 10 ps, the measured ripple depth is about 194 nm, but it is decreased to about 169 nm at the large time delay of Δt_2 = 60 ps. Generally speaking, the above phenomena are much different from the observations by only using two time-delayed femtosecond laser pulse with different polarizations in our previous study [36].

In addition, we also investigated the time delay dependence of the slanting ripple orientation angle under the condition of Δt_1 = 60 ps. In this case, the temporal separation between the incident laser beams P_1 and P_2 becomes relatively large. As shown in Fig. 5(d), with increasing the second time delay in a range of Δt_2 = 0-60 ps, the measured slanting degree of the ripple orientation presents a rapidly rising tendency followed by an evident dropping trend. Quite different from the observation in Fig. 5(a), however, the obtained peak value of the slanting degree for the ripple orientation is as large as approximately α = 60°, whose corresponding second time delay is blue-shifted to Δt_2 = 15 ps. This means that the ripple orientation can be varied within a large range, even perpendicular to the direction of the linear polarization of the femtosecond laser beam P_1. In this case, the ripple orientation is similar to the observation in Fig. 2(a), but with a different spatial period.

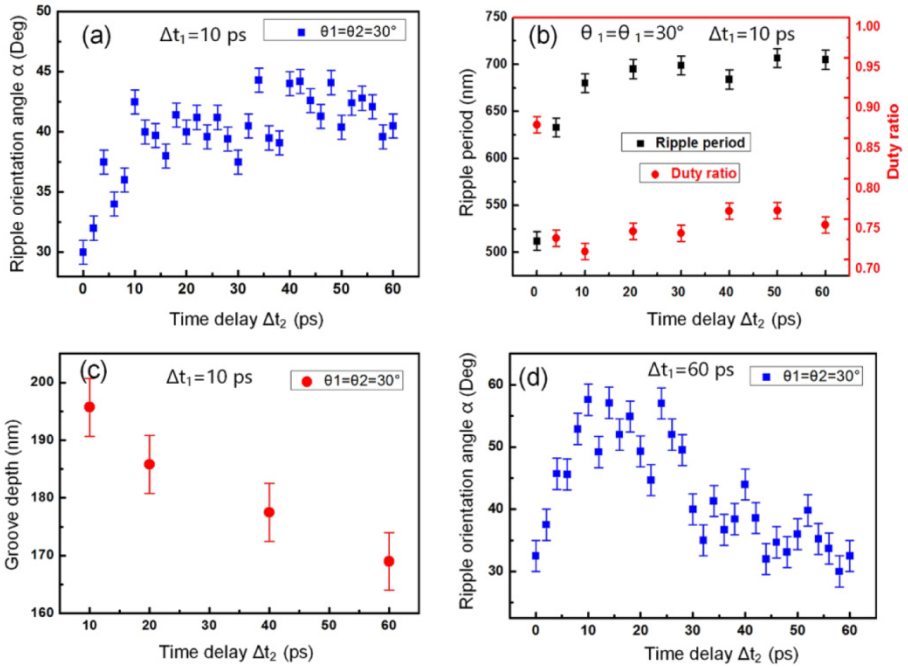

Fig. 5. (a)-(c) Measured ripple orientation angle, spatial period and the duty ratio, and groove depth as a function of the second time delay Δt_2, respectively, with three time-delayed femtosecond laser beams irradiating on the surface of 4H-SiC crystal, where the time delay Δt_1 is fixed at 10 ps; (d) Measured second time delay (Δt_2) dependence of the ripple orientation angle at the fixed time delay Δt_1 = 60 ps. In all these cases the intersection angles among three laser polarizations are $\theta_1 = \theta_2 = 30°$.

To elucidate the underlying mechanisms of the experimental observations, we try to propose a physical scenario as follows: when single-beam femtosecond laser pulses irradiate the sample at the high peak fluence of 0.24 J/cm^2, the formation of the HSF ripple structures

Optics EXPRESS

is commonly attributed to the spatially periodic ablation of the material by the interference between the incident light and its excited SPP, and thus the ripple period is determined by the excited dielectric constant on the material surface [12]. However, for the experiments of three time-delayed femtosecond laser pulses, when the first femtosecond laser pulse (of the beam P_1) strikes the semiconductor, a high-density free-electron plasma is generated in the laser-exposed surface region via multi-photon absorption process [32]. Subsequently, the laser-SPP interference can produce spatially periodic energy depositions to transiently modulate the material optical properties, leading to the emergence of a refractive index metasurface with a grating vector $\mathbf{k}_{1g}$ parallel to the direction of the electric field E_1 [37]. During the relaxation processes of such a transient surface pattern, if the second femtosecond laser pulse (of the beam P_2) with the linear polarization different from E_1 arrives, its wave vector $\mathbf{k}_{20}$ projected on the sample surface displays an azimuth angle of θ_1 with respect to the transient grating vector $\mathbf{k}_{1g}$. According to the law of conversation of momentum, this kind of non-collinear alignment reasonably causes the excitation of surface waves ($\mathbf{k}_{2sw}$) in a new direction [38], Therefore, another periodic pattern of the transient refractive index is developed with the grating vector $\mathbf{k}_{2g}$ (actually in two opposite directions). Similarly, we can consider that the above process also provides a new transient index metasurface for the time-delayed incident third femtosecond laser pulse (of the beam P_3) linearly polarized in another direction, and their physical coupling at an azimuth angle of θ_2 consequently affects the excitation of surface waves along the direction of $\mathbf{k}_{3sw}$, whose spatially periodic ablation of the material with near-field localized high intensity results in the formation of the permanent periodic ripple structures on the sample surface. Specifically, the obtained ripple orientation becomes perpendicular to the direction of $\mathbf{k}_{3sw}$ rather than only determined by the direction of the linear polarization of the individual laser pulses. The above mentioned physical processes are shown by a schematic diagram in Fig. 6(a).

For a given time delay Δt_1 between the femtosecond laser pulse beams P_1 and P_2, the spatial alignment of the transient grating vector $\mathbf{k}_{2g}$ becomes determined. However, its magnitude tends to change with the time delay between two femtosecond laser beams P_2 and P_3 because of its geometric dynamics, which can be described as [39]:

$$k_{2g} = k_{20}\sqrt{1+\frac{a^2}{d^2}\tan^2(k_{20}h)} \tag{1}$$

where *a, d* and *h* are the excited stripe width, the period, and the depth of the transient index grating, respectively. More specifically, the temporal evolution of a spatial volume of each transient index stripe heated by the laser intensity fringe first increases and then decreases via both the electronic diffusion and electron/coupling processes [40], which results in a growing-up-and-shortening variation for the magnitude of $\mathbf{k}_{2g}$, and so does the direction of the wave vector $\mathbf{k}_{3sw}$. This is probably the reason for the observed slanting behaviors of the ripple orientation in Fig. 5(a). On the other hand, for the larger time delay Δt_1 = 60 ps, as shown in Fig. 6(b), the lattice heated by the laser beam P_1 can reach the higher temperature, therefore, the spatial volume of each stripe in the transient index grating induced by the laser beam P_2 is varied within a large dynamic range. Correspondingly, the magnitude of the grating vector $\mathbf{k}_{2g}$ becomes easily modulated, leading to a dramatic change in the direction of $\mathbf{k}_{3sw}$ and its resultant slanting degree of the ripple orientation, which is in accordance with the observation in Fig. 5(d).

The observed ripple orientation at the second time delay Δt_2 = 0 ps can be understood as follows: Upon irradiation of the first femtosecond laser pulse P_1, a transient index grating is created on the surface of SiC crystal with the grating vector $\mathbf{k}_{1g}$ parallel to the direction of incident laser polarization. When the laser pulses P_2 and P_3 spatiotemporally irradiate the sample surface, their optical interference results in an elliptical polarization with the major axis of the electric field along the direction close to the wave vector $\mathbf{k}_{20}$, which subsequently

Optics EXPRESS

excites the surface plasmon on the transient metasurface of $\mathbf{k}_{1g}$ in the same direction. As a result, the eventually obtained periodic ripple structures are shown to have orientation almost perpendicular to the laser polarization P_2.

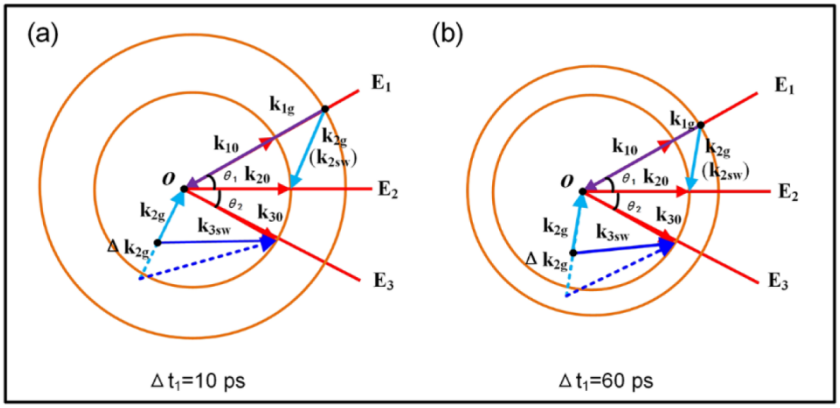

Fig. 6. Proposed physical model for slanting orientation of the ripple structures formed on the surface of 4H-SiC crystal upon irradiation of three time-delayed femtosecond laser pulse beams linearly polarized in different directions. (a) In the case of Δt_1 = 10 ps; (b) In the case of Δt_1 = 60 ps. Here $\mathbf{k}_{10}$, $\mathbf{k}_{20}$ and $\mathbf{k}_{30}$ are the wave vectors of the laser beams P_1, P_2 and P_3 projected on the sample surface, respectively; $\mathbf{k}_{1g}$ and $\mathbf{k}_{2g}$ are the grating vectors of the transient index metasurfaces induced by the laser beams P_1 and P_2, respectively; $\Delta\mathbf{k}_{2g}$ is a time-dependent variation in the magnitude of $\mathbf{k}_{2g}$.

In order to confirm the above assumptions, we also carried out further experiments by changing the polarization intersection angles of three laser beams to other values such as $\theta_1 = \theta_2 = 45°$. Very similar to the observations in $\theta_1 = \theta_2 = 30°$, the available surface structures also display the uniform LSF ripple morphology, especially when the second time delay is varied within a range of Δt_2 = 10-40 ps, as shown in Fig. 7, where the first time delay is maintained at Δt_1 = 10 ps. Under such circumstances, a quantitative description of the time delay dependent ripple orientation angle is illustrated in Fig. 8(a). Clearly, the ripple orientation induced at the time delay Δt_2 = 0 ps is about $\alpha = 45°$, which is almost perpendicular to the direction of the linear polarization of the laser beam P_2. Remarkably, the maximum slanting degree of the ripple orientation can reach as large as $\alpha = 80°$ at Δt_2 = 12 ps. Afterwards, the measured slanting degree begins to slowly decrease down to about $\alpha = 62°$ at Δt_2 = 60 ps.

Optics EXPRESS

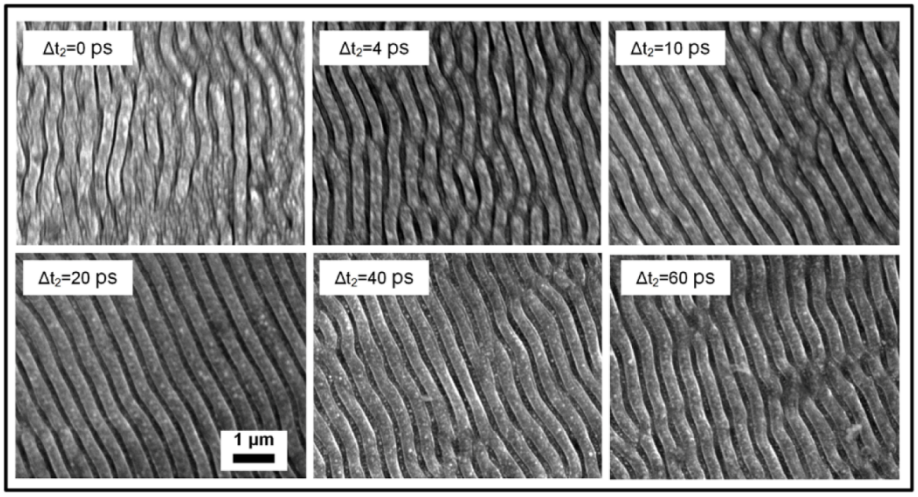

Fig. 7. Observed LSF ripple structures on the surface of 4H-SiC crystal induced by three femtosecond laser pulse beams with several time delays of Δt_2, where other laser parameters are adopted as $\theta_1 = \theta_2 = 45°$ and $\Delta t_1 = 10$ ps.

With three linearly polarized femtosecond laser beams, we also investigated the second-time-delay dependent slanting ripple orientation under the condition of larger value of Δt_1 = 60 ps, and the corresponding result is shown in Fig. 8(b). It is found that the peak slanting degree is increased to about $\alpha = 90°$, which means that the slating degree becomes more pronounced with larger polarization intersection angles of three laser beams, but the maximum slanting orientation appears to be always near perpendicular to the direction of the linear polarization of the laser beam P_1. On the other hand, when the second time delay Δt_2 is more than 12 ps, a rapid decreasing tendency with a large dynamic range is achieved. Undoubtedly, such phenomena indicate the formation of the slanting ripple structures is essentially related to transient dynamic properties of the sample surface excited by two pre-incident femtosecond laser pulses, and they can be satisfactorily explained with the help of the aforementioned theoretical model.

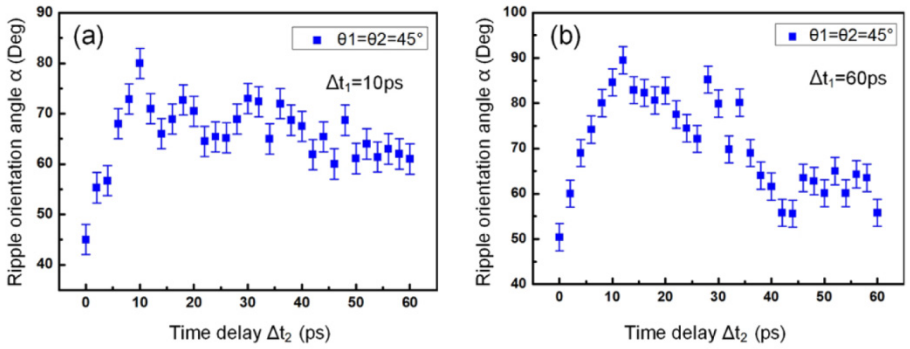

Fig. 8. Measured ripple orientation angles as a function of the second time delay Δt_2 for the irradiation of three time-delayed femtosecond laser pulse beams on the surface of 4H-SiC crystal, where the polarization intersection angles of three laser beams are $\theta_1 = \theta_2 = 45°$. (a) Δt_1 = 10 ps; (b) Δt_1 = 60 ps.

To understand the LSF features of the ripple structures on the semiconductor surface induced by three time-delayed femtosecond laser beams, we consider the physical origins of the ripple formation, which is believed to be due to the interference between the incident light

Optics EXPRESS

and the excited surface wave. Based on this approach, the ripple period can be expressed as follows [12]:

$$\Lambda = \lambda(\frac{1}{\varepsilon_d} + \frac{1}{\varepsilon_m})^{1/2} \quad (2)$$

where ε_d and ε_m are the dielectric constants of the ambient medium and the excited sample surface, respectively. For the irradiation of a high-fluence single femtosecond laser beam, the ambient air medium is known as $\varepsilon_d = 1$ and ε_m tends to be largely negative, which makes an item value in the bracket of Eq. (2) always much less than 1. This corresponds to the ripple structures with the traditional HSF features [in Fig. 2]. As for the situation of three time-delayed femtosecond laser beams, when the first laser pulse (of the beam P_1) irradiates the sample surface, free electrons are generated in the laser exposed region via multi-photon absorption process, part of which can escape out of the target to produce a thin layer of plasma localized on the sample surface. Under such circumstances, the ripple structures are unable to form because of the lower peak fluence, however, the transient dielectric constant of the ambient air medium is reduced (still with a positive value less than 1), which can be described by $0 < \varepsilon_d = 1 - \frac{\omega_p^2}{\omega^2 + \gamma^2} < 1$ [41], where $\omega_p \sim N_e^{1/2}$ is the electron density (N_e) dependent plasma frequency, ω for the incident laser frequency, γ for the electron collision frequency. Similarly, if the second delayed femtosecond laser pulse (of the beam P_2) arrives on the sample surface during the lifetime of this thin plasma, the density of the free electrons will be enhanced to further decrease the dielectric constant of ambient air medium. Consequently, when the third delayed femtosecond laser pulse (of the beam P_3) reaches the sample surface, the item value in the bracket of Eq. (2) possibly becomes increased due to the smaller ε_d, leading to the large ripple period. Namely, it is the transient optical changes simultaneously occurring in both the ambient air medium and on the semiconductor surface that promotes the growth of the LSF structures. In fact, this kind of behavior is also believed to affect other physical properties of the material during the nonequilibrium dynamic processes, which eventually improves the spatial distribution quality of the ripple formation.

4. Conclusions

To conclude, we have reported a new method based on exploiting three temporally delayed femtosecond laser pulse beams collinearly propagated with different linear polarizations for the control of the periodic ripple structures on the semiconductor 4H-SiC crystal surface. It has been experimentally found that the induced ripple orientation, which is neither perpendicular nor parallel to any laser polarizations, is slanted with regard to the situation by the individual irradiation of the final delayed high-energy laser pulse, and its slanting degree is non-monotonically changed with time delays. A variation range of the slanting degree is evidenced to increase for larger polarization intersection angles of three laser beams. Meanwhile, the ripple period of such surface structures is shown to be capable of switching from the semi-disordered HSF distribution to the uniform distinct LSF arrangement accompanied by broadening the groove width, which is very like the observations on metals. These special features, primarily the ability to process the ripple formation, are nominally not achievable with conventional one- or two-pulse laser beam irradiation.

In theory, we have proposed a physical model by recognizing the correlated interactions of three femtosecond laser pulses via transient surface dynamics to explain the experimental phenomena: Upon irradiation of the first laser pulse, a transient index grating is generated on the surface due to the interference of the incident laser with the excited surface wave, and its emergence and relaxation subsequently influences the surface wave excitation of the second delayed incident femtosecond laser pulse to produce another transient index grating with the modified grating vector. Accordingly, for the delayed incident third femtosecond laser pulse,

Optics EXPRESS

the direction of its surface wave excitation is certainly deviated by the transient index metasurface, whose resultant periodically distributed energies eventually lead to the permanent ripple structures with the slantwise orientation. In addition, the formation of LSF ripple structures is attributed to changes in the dielectric constant of both the sample and the ambient air medium owing to the laser excitation. The theoretical interpretations agree with the experimental observations, and they are also supported by the further experiments. In principle, our technique is not only limited to SiC crystal and can be applied to other semiconductor materials. Our investigations give deep insights into the physics of the laser-material interaction and find a new way to effectively control ripples via transient surface dynamics, which is very important for the potential applications in laser direct fabrication of micro/nano-devices.

Funding

Natural National Science Foundation of China (NSFC) (11274184, 11674178); Tianjin National Natural Science Foundation (12JCZDJC20200); Research Fund for the Doctoral Program of higher Education of China (20120031110032).